

PAPER • OPEN ACCESS

A digitally printed optoelectronic nose for the selective trace detection of nitroaromatic explosive vapours using fluorescence quenching

To cite this article: N Bolse *et al* 2017 *Flex. Print. Electron.* 2 024001

View the [article online](#) for updates and enhancements.

Related content

- [Detection of nitroaromatics in the solid, solution, and vapor phases using silicon quantum dot sensors](#)
An Nguyen, Christina M Gonzalez, Regina Sineinikov *et al.*
- [Chemosensors for detection of nitroaromatic compounds \(explosives\)](#)
G V Zyryanov, D S Kopchuk, I S Kovalev *et al.*
- [Fluorescent film sensor for nitroaromatics](#)
Jianping Kang, Liping Ding, Fengting Lü *et al.*

Recent citations

- [Ormosil-coated conjugated polymers for the detection of explosives in aqueous environments](#)
Ross N. Gillanders *et al*
- [Semiconductor/Insulator Blends for Speed Enhancement in Organic Photodiodes](#)
Noah Strobel *et al*
- [Lab-on-Chip, Surface-Enhanced Raman Analysis by Aerosol Jet Printing and Roll-to-Roll Hot Embossing](#)
Anne Habermehl *et al*

Flexible and Printed Electronics



PAPER

A digitally printed optoelectronic nose for the selective trace detection of nitroaromatic explosive vapours using fluorescence quenching

OPEN ACCESS

RECEIVED
15 September 2016

REVISED
24 February 2017

ACCEPTED FOR PUBLICATION
10 March 2017

PUBLISHED
24 April 2017

Original content from this work may be used under the terms of the [Creative Commons Attribution 3.0 licence](#).

Any further distribution of this work must maintain attribution to the author(s) and the title of the work, journal citation and DOI.



N Bolse¹, R Eckstein^{1,2}, M Schend¹, A Habermehl¹, C Eschenbaum^{1,2,3}, G Hernandez-Sosa^{1,2} and U Lemmer^{1,2,3}

¹ Light Technology Institute, Karlsruhe Institute of Technology (KIT), Engesserstrasse 13, D-76131 Karlsruhe, Germany

² InnovationLab, Speyerer Str. 4, D-69115 Heidelberg, Germany

³ Institute of Microstructure Technology, Karlsruhe Institute of Technology (KIT), Hermann-von-Helmholtz-Platz 1, D-76344 Eggenstein-Leopoldshafen, Germany

E-mail: nico.bolse@kit.edu

Keywords: aerosol-jet printing, fluorescence quenching, optoelectronic nose, nitroaromatic explosives, vapour detection, pattern recognition, sensor arrays

Supplementary material for this article is available [online](#)

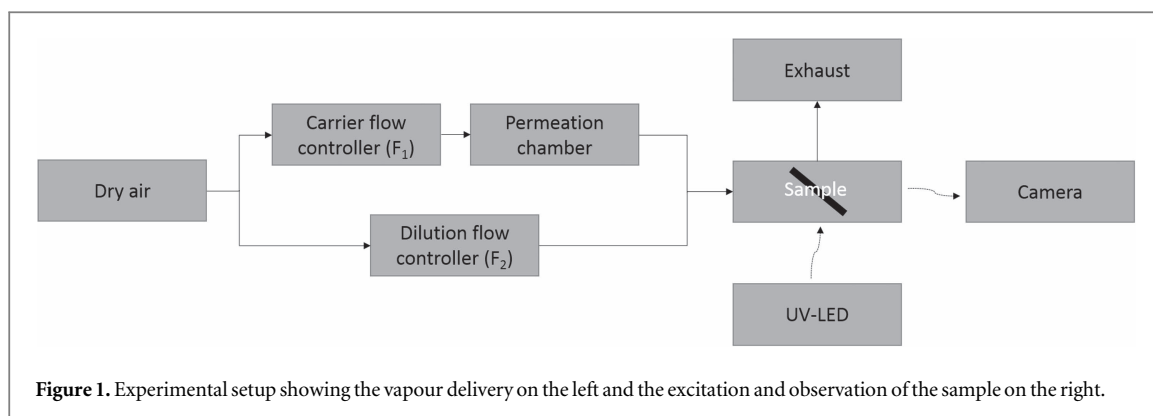
Abstract

We report on a fluorescent optoelectronic nose for the trace detection of nitroaromatic explosive vapours. The sensor arrays, fabricated by aerosol-jet printing, consist of six different commercially available polymers as transducers. We assess the within-batch reproducibility of the printing process and we report that the sensor polymers show efficient fluorescence quenching capabilities with detection limits of a few parts-per-billion in air. We further demonstrate the nose's ability to discriminate between several nitroaromatics including nitrobenzene, 1,3-dinitrobenzene and 2,4-dinitrotoluene at three different concentrations using linear discriminant analysis. Our approach enables the realization of highly integrated optical sensor arrays in optoelectronic noses for the sensitive and selective detection of nitroaromatic explosive trace vapours using a potentially low-cost digital printing technique suitable for high-volume fabrication.

1. Introduction

With increasing worldwide security concerns, research on optical fluorescent sensors for the trace detection of nitroaromatic explosives has become increasingly important [1–3]. The low detection limits render fluorescence quenching a promising approach [4–6]. Sensor systems based on fluorescence quenching can be low-cost and portable alternatives for established approaches such as the expensive and bulky ion mobility spectroscopy or as the assignment of explosives detection dogs that require high training costs without providing twenty-four-seven availability [7]. However, a single optical sensor typically lacks selectivity that can be overcome with sensor arrays. These arrays represent an optoelectronic nose if equipped with pattern recognition methods for the discrimination between various explosives and interferents [8–14].

The detection limits of such noses need to be as low as a few parts-per-billion (ppb) in order to be competitive. Here, amplifying fluorescent polymers have recently shown excellent sensing properties among other materials [15–22]. The interaction of these polymers with electron deficient nitroaromatic species typically leads to a photo-induced electron transfer (PET) that quenches the polymer's fluorescence. Moreover, Förster resonance energy transfer (FRET) and Dexter energy transfer (DET) can cause a quenching of the fluorescence, too. However, FRET requires an energetic overlap of the polymer emission with the nitroaromatic absorption and DET is typically observed at high target concentrations only [23]. The main advantage of amplifying fluorescent polymers relative to single chromophores is the long exciton migration path enhancing the probability of excitons interacting with binding sites occupied by nitroaromatic species. Rigid three-dimensional



structures in combination with long twisted polymer backbone galleries further enhance the sensing performance as they offer interchain spacing. This spacing allows for an efficient binding of nitroaromatic species while preventing self-quenching [24]. Polymers with such properties, however, typically require complex synthesis often being unattractive for commercial applications. This might be problematic for the incorporation of multiple polymers into an optoelectronic nose required to enable selectivity among different target analytes [25].

Here, in contrast, we report on the development of sensitive and selective sensor arrays employing off-the-shelf polymers without special three-dimensional structures. So far, these polymers have been typically used in other applications such as organic light-emitting diodes [26–29], organic lasers [30–32], organic electroluminescent cells [33] and organic light-emitting transistors [34]. More importantly, we show the digital printability of these polymers by aerosol-jet (AJ) printing to realize reproducible optoelectronic noses for the sensitive and selective trace detection of nitroaromatic explosive vapours. In contrast to spin-coating and other solution-processing techniques such as doctor blading and dip coating, printing enables user-defined structures that can be highly integrated when deposited from nozzles with μm -orifices. The high throughput offered by roll-to-roll machines further allows fabrication upscaling towards mass-produced low-cost optoelectronic noses aiming at commercial applications. Here, reproducibility becomes even more important so that only a subset of noses need to be trained with pattern recognition methods per batch.

2. Materials and methods

2.1. Target analytes

In this study, the nitroaromatic analytes nitrobenzene (NB), 1,3-dinitrobenzene (DNB) and 2,4-dinitrotoluene (DNT) were used as target analytes. These compounds are often used for the manufacture of explosives making them favourable detection candidates in security related sensing [35]. For example, DNT residues are typically found in 2,4,6-trinitrotoluene (TNT). However, DNT's

vapour pressure is one order of magnitude larger as compared to TNT. Therefore, DNT is usually sensed when technical sensors or explosives detection dogs detect TNT [36, 37]. In addition to the nitroaromatic analytes, we investigated the detectability of benzophenone (BP) as a control substance due to its aromatic structure with high electron-affinity but without nitro groups. Each target analyte was purchased as a high-emission permeation tube from Macherey-Nagel GmbH & Co.KG and used as received. Their molecular structures are provided in the supporting information S1 available online at stacks.iop.org/FPE/2/024001/mmedia.

2.2. Sensor materials

Our sensor arrays consist of four commercial polymers from Merck LiviluxTM and two commercial polymers from American Dye Source. The Merck polymers include PDY-132 (SY), SPG-01T (PG), SPB-02T (PB) and SPW-111 (PW). American Dye Source supplied ADS229BE (PFO) and ADS133YE (F8BT). More information on the materials is provided in the supporting information S3–S7. The sensor polymers were dissolved in toluene with a concentration of 1 g l^{-1} each. To enable printability in the AJ printer (AJ-300, Optomec), 50% of the high-boiling solvent 1,2,3,4-tetrahydronaphthalene (tetralin) was added to the polymer solutions. Then an aerosol stream carrying the corresponding atomized polymer solution was directed through the printer's nozzle and deposited onto a glass slide substrate that had been plasma treated before. The AJ printer was employed with a $200\text{ }\mu\text{m}$ nozzle using a shutter time of 1 s to print twelve 2×3 arrays onto the substrate.

2.3. Experimental setup

A block diagram of the experimental setup for the delivery of target analyte vapours and for the measurement of fluorescence intensities is shown in figure 1.

A permeation-based vapour generator (Dynacalibrator 235, Vici) was used to deliver constant vapour concentrations in a stream of dry air (0%rH). The target analytes showed a stable permeation through the tubes for a constant permeation chamber temperature. The vapour concentration was adjusted by

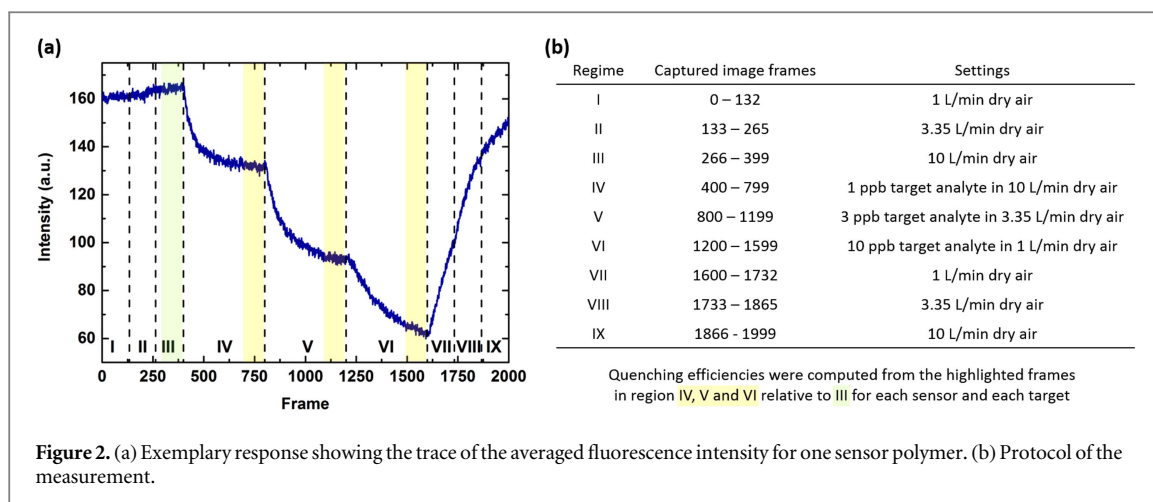


Figure 2. (a) Exemplary response showing the trace of the averaged fluorescence intensity for one sensor polymer. (b) Protocol of the measurement.

diluting the carrier flow in the permeation chamber. Details on the generation of different concentrations are given in the supporting information S2. We used a 365 nm light emitting diode (M365L2, Thorlabs) with collimating optics to excite the fluorescence with a power between 6 and 160 μW across the full area of the $26 \times 26 \text{ mm}^2$ substrate from the backside. The excitation power was measured using a coherent fieldmaster with an LM-2 UV detector head. A CCD-camera (DFK21BU618, the imaging source) with a resolution of 640×480 was mounted with a Ricoh FL-CC2514-2M lens (focal length 25 mm, iris 1.4, spacing rings) behind a UV-filter to capture YUY2-formatted images of the sensor arrays at a framerate of 0.5 FPS using a camera exposure time of 0.5 s with a gain of 947. The samples were tilted relative to the camera at an angle of 30° . The camera measured the average fluorescence intensities emitted from the sensor polymers. Therefore, the regions of interest were evaluated in a rectangle of 5×5 pixels in the centre of each printed sensor polymer. The signals were averaged over twelve arrays leading to a total number of 300 pixels considered for each average sensor intensity. The fluorescence was background corrected and measured at room temperature.

2.4. Measuring the fluorescence quenching

An exemplary measurement sequence is depicted in figure 2 showing the response of the polymer PW to DNT. As the vapour concentration had to be adjusted by three different dilution flows, a flow-dependency test was performed at the beginning of the experiments. Here, the fluorescence was measured in air at the three flow rates (regimes I, II and III). In some cases, the quenched signals did not saturate completely at the end of the quenching regimes (IV, V and VI). This can be attributed to relatively thick sensor layers allowing for a diffusion of the target analytes deep into the sensor layers (see figure 3). Therefore, the quenching for each concentration was evaluated after constant time intervals. The sensor arrays were purged with dry air at the end of the experiment (regimes VII,

VIII and IX) at the same flow rates to allow for the investigation of the sensor array recovery.

2.5. Analysing the fluorescence quenching patterns

For the sensor arrays, linear discriminant analysis (LDA) was used to investigate the potential ability of the optoelectronic nose to discriminate between target analytes at different concentrations. The LDA was employed as a supervised statistical learning method maximizing the ratio of between-class to within-class variation [38]. Here, each target analyte at a fixed concentration represented a class. The corresponding fluorescence quenching (as taken from the highlighted areas of the regimes IV, V and VI in figure 2 for each polymer) was used to derive the linear discriminant functions that enable separation. Typically, most of the between-class variance is contained in a few discriminant functions only, allowing for a reduction of the data dimensionality. Wilks' lambda was used to test the significance of the linear discriminant functions [39]. The parameter measures if a class mean projected by the tested discriminant functions differs from other class means. The smaller the Wilks' lambda the higher is the difference between classes. Furthermore, the fluorescence quenching was checked for normality and for the equality of covariance, both of which are theoretical requirements for the LDA. Normality was tested with a χ^2 quantile quantile (QQ) graph that plots the observed quantiles (ascendingly sorted Mahalanobis distances of each LDA data point to its class mean in squared units) versus the expected quantiles (inverse of the χ^2 cumulative distribution) [40]. The equality of covariance was checked using a Bartlett test [41]. In practice however, LDA is often applied when the conditions of normality and the equality of covariance do not hold. In these cases, a separation of classes is often possible, but will not be optimal. The LDA model was assessed with common validation techniques such as leave-one-out and subset validation. The former method is a K -fold cross validation where K equals the number of observations. The latter method divides the data into two randomly

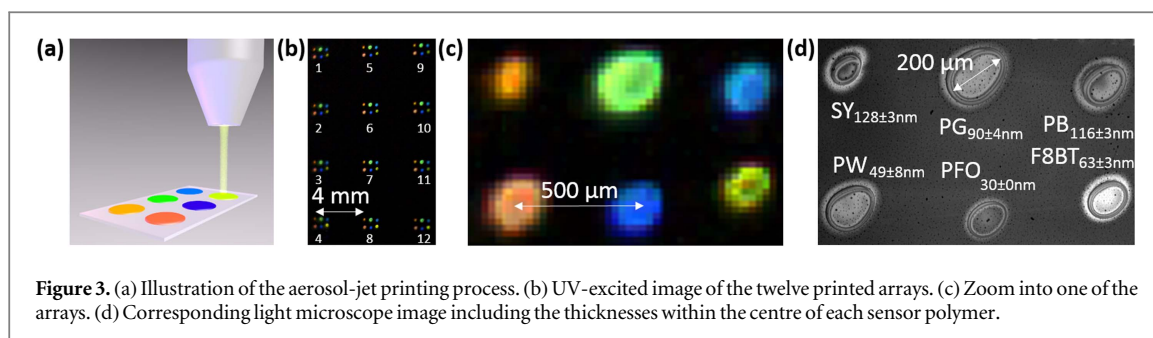


Figure 3. (a) Illustration of the aerosol-jet printing process. (b) UV-excited image of the twelve printed arrays. (c) Zoom into one of the arrays. (d) Corresponding light microscope image including the thicknesses within the centre of each sensor polymer.

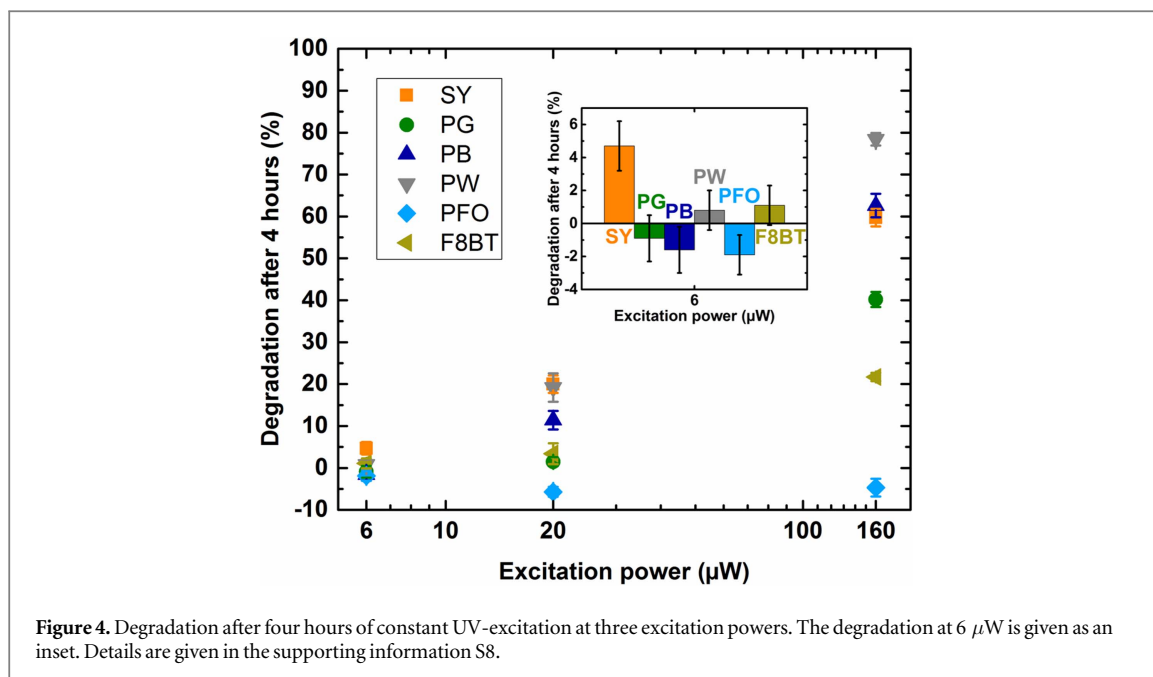


Figure 4. Degradation after four hours of constant UV-excitation at three excitation powers. The degradation at 6 μW is given as an inset. Details are given in the supporting information S8.

but normally sorted subsets. One set is used for training while the LDA predicts the classes for the remaining set. Thus, both methods measure the robustness against out-of-sample observations.

3. Results and discussion

3.1. Fabrication analysis

The six polymers were deposited using AJ printing illustrated in figure 3(a). In total, twelve 2×3 arrays were printed onto a substrate with a pitch of 4 mm as shown in figure 3(b). The four arrays in the middle appear sharper as compared to the left and right because the sample holder had to be tilted relative to the camera. This shifted the outer columns slightly out of focus (see figure 1). However, the later discussed low standard deviations for the quenching show that it did not affect the relative fluorescence intensities. Figure 3(c) shows a zoom into one of the UV-excited arrays. Each individual sensor polymer had a pitch of roughly 500 μm. The printed structures formed plateaus surrounded by rings with a maximum diameter of roughly 200 μm ('coffee staining'). These rings were up to 500 nm in height because of the drying process. However, the thickness of the plateaus was

homogeneous as measured with a Bruker Dektak XT profilometer for four different arrays. Due to the low thickness deviations given in figure 3(d), we conclude that the plateaus can be printed reproducibly.

3.2. Degradation analysis

As light emitting polymers typically suffer from photo bleaching, the optically induced degradation of the nose was investigated first. Therefore, the sensor arrays were excited at three different powers for 4 h in a stream of dry air at 1 l min^{-1} . Equation (1) defines the degradation D .

$$D = \frac{I_{\text{start}} - I_{\text{end}}}{I_{\text{start}}}. \quad (1)$$

For each sensor polymer, I_{start} denotes the average fluorescence intensity of the first 100 frames right after the measurement was started and I_{end} denotes the average fluorescence intensity of the last 100 frames right before the 4 h had passed. Figure 4 depicts this degradation versus the excitation power. The error bars represent the standard deviations within the twelve arrays.

With the exception of PFO, the sensor polymers strongly suffer from photo bleaching at high excitation powers. However, the degradation for a power of

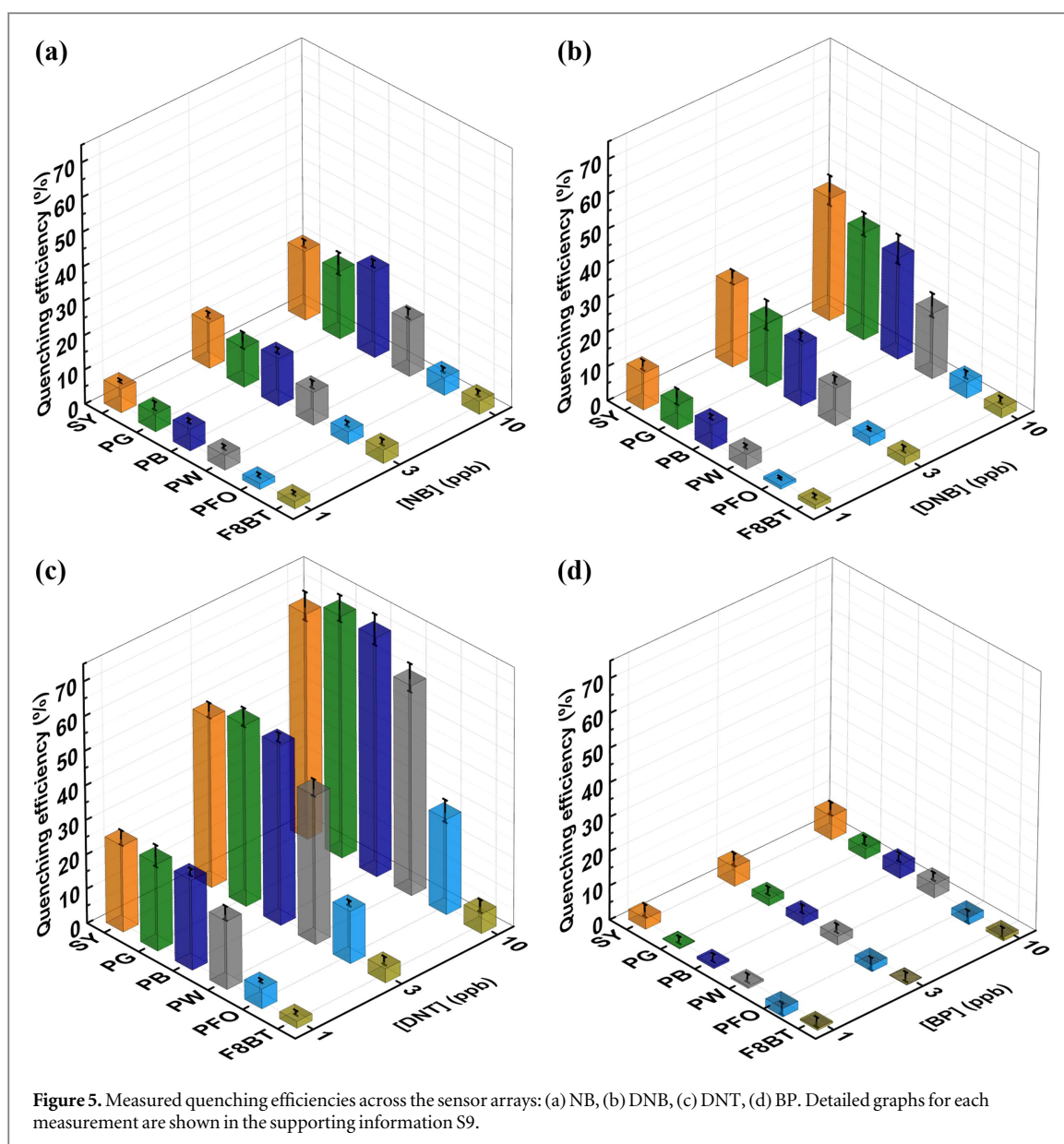


Figure 5. Measured quenching efficiencies across the sensor arrays: (a) NB, (b) DNB, (c) DNT, (d) BP. Detailed graphs for each measurement are shown in the supporting information S9.

$6 \mu\text{W}$ is negligible. Only SY seems to degrade slightly within the 4 h. To reduce sensor drifts, we therefore used an excitation power of only $6 \mu\text{W}$. As a trade-off, the camera exposure time had to be increased from 5 ms at $160 \mu\text{W}$ or 125 ms at $20 \mu\text{W}$ respectively to 500 ms at $6 \mu\text{W}$ for a sufficient fluorescence brightness.

3.3. Quenching efficiency analysis

The quenching efficiencies were determined from the last 100 frames of each quenching regime (IV, V and VI) relative to the last 100 frames in air (regime III) as described in figure 2. Hereby, a large number of observations was provided for the later discussed discriminant analysis allowing for the estimation of how the patterns scatter due to noise and due to unsaturated quenching. Equation (2) shows the definition of the quenching efficiency QE.

$$\text{QE} = \frac{I_0 - I_q}{I_0}. \quad (2)$$

Here, I_0 is the average intensity of the considered data points in air and I_q is the average quenched intensity of the considered data points at a constant target concentration. The average quenching efficiency patterns of the sensor arrays for the four investigated analytes between 1 and 10 ppb are shown in figure 5. The error bars represent the standard deviations within the twelve arrays.

There are distinct QE patterns caused by the interaction of the sensor polymers with each target analyte. The extent of the fingerprints increases with concentration up to quenching efficiencies of almost 70% for 10 ppb DNT. In contrast, BP seemed not to quench the fluorescence. To discuss potential quenching mechanisms, the absorption and emission spectra and the energies for the highest occupied molecular orbital (HOMO) and for the lowest unoccupied molecular

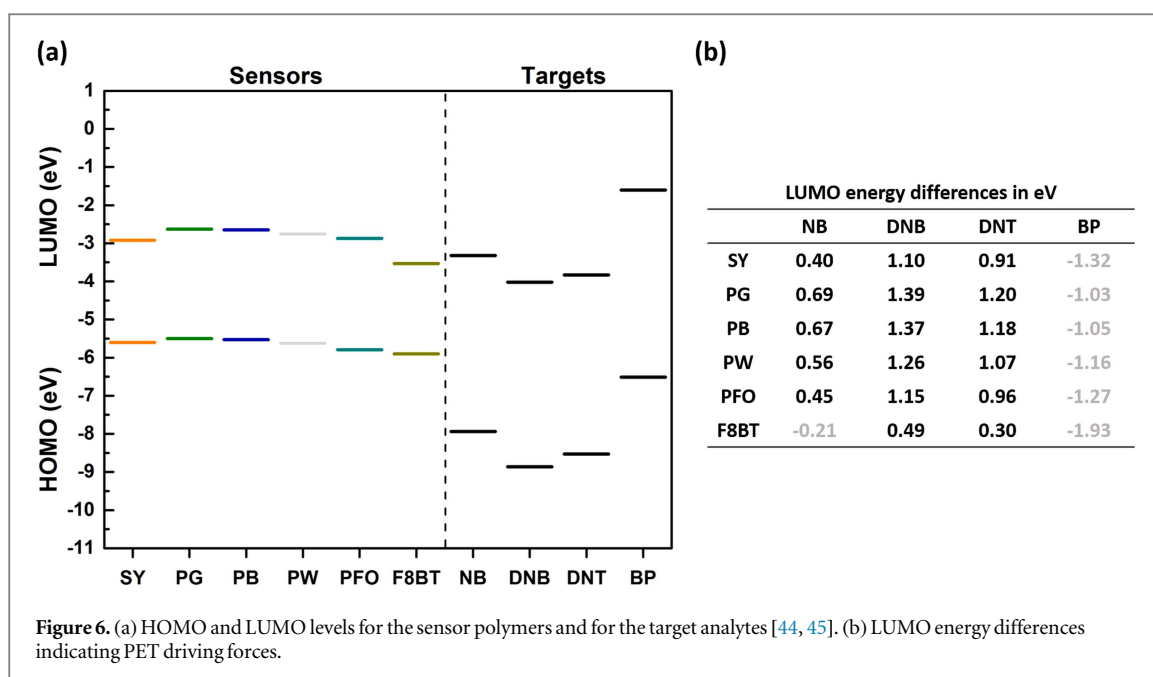


Table 1. Minimum, mean and maximum standard deviation of the quenching efficiencies for each sensor polymer considering all target analytes and concentrations.

QE standard deviations in %	SY	PG	PB	PW	PFO	F8BT
Minimum	0.48	1.03	0.62	0.62	0.36	0.60
Average	2.03	2.51	1.59	1.73	1.15	1.07
Maximum	4.35	4.29	4.48	4.10	3.28	1.79

orbital (LUMO) were measured from thin film samples. Details are provided in the supporting information S5–S7. A comparison of the sensor polymer emission spectra as given in the supporting information figure S2 with the target analytes absorption spectra as given in [42, 43] indicates that FRET did not contribute to the quenching. Moreover, DET is negligible at these low concentrations. Instead, PET could have caused the quenching if there is a positive driving force between the LUMOs of the sensor polymers and the target analytes. Therefore, figure 6 depicts the estimated polymer LUMOs and PET driving forces. HOMO and LUMO energies for the target analytes were taken from literature [44, 45].

There is indeed a positive PET driving force between most of the sensor polymers and target analytes. In conclusion, we attribute the quenching to a dominant PET process. The strongest driving forces result from the LUMO of SY, PG, PB, PW and PFO to the LUMO of the electron deficient nitroaromatics DNB and DNT. The driving force to NB is much weaker. This is consistent with the smaller quenching efficiencies caused by NB. For F8BT, there is only a weak driving force to DNB and DNT while there is no driving force to NB. BP cannot be detected by any of the sensor polymers due to its high LUMO, which is consistent with the measurements. This confirms that the sensor array is not responding arbitrarily to

any kind of target class but rather responds selectively to the class of nitroaromatics. Furthermore, it supports the assumption of PET as the dominant quenching mechanism due to the energetic configuration. However, the order of the quenching efficiencies disagrees to some extent with the order of the driving forces ($QE_{PG} > QE_{PB} > QE_{PW} > QE_{PFO} > QE_{SY} > QE_{F8BT}$ and $QE_{DNB} > QE_{DNT} > QE_{NB} > QE_{BP}$). A possible explanation is the role of different adsorption efficiencies for each combination of target analyte and sensor polymer as discussed in [46] or different diffusion and binding properties of the vapours which have recently been found to play the first-order roles in the fluorescence quenching process instead of amplification through long exciton migration paths [47, 48]. This would further increase the unambiguousness of the response patterns.

To investigate the reproducibility of the printed arrays, the standard deviations of the quenching efficiencies from all sensor arrays over all measurements are shown in table 1. The low deviations validate the fluorescence responses and thus demonstrate the reproducible within-batch fabrication.

The recovery of the sensor arrays can be investigated from the regimes VII, VIII and IX as described in figure 2. Overall, we observed a limited recovery due to the relatively thick sensor layers allowing for a deep diffusion of the target analytes into the sensor polymers. After a strong purge at the end of the regime IX, most sensor polymers had recovered 60%–100% of their initial fluorescence depending on the target analyte. However, as the printing process potentially enables the fabrication of low-cost sensor arrays in high volumes, disposable detector cards can be used in potential field applications. No recovery abilities are required in this case. Details for the recovery are given in the supporting information S10.

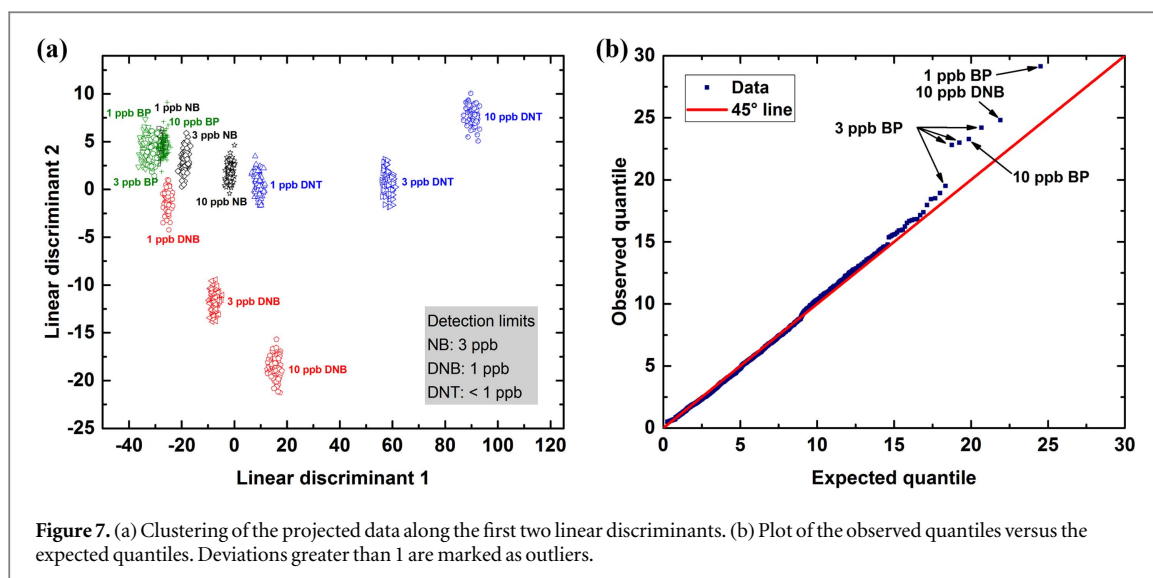


Figure 7. (a) Clustering of the projected data along the first two linear discriminants. (b) Plot of the observed quantiles versus the expected quantiles. Deviations greater than 1 are marked as outliers.

Table 2. Eigenvalues and explained variance for the linear discriminant functions.

Linear discriminant	Eigenvalue	Variance explained	
		(%)	Cumulative (%)
1	1395.9	95.40	95.40
2	53.2	3.63	99.03
3	10.4	0.71	99.74
4	2.3	0.16	99.90
5	1.1	0.07	99.97
6	0.4	0.03	100.00

3.4. Pattern analysis

LDA was used to maximize the ratio of between-class to within-class variation of the multidimensional sensor array signals. Therefore, the quenching efficiencies of the six sensor polymers in the twelve arrays were used to derive the linear discriminant functions enabling the clustering of the labelled data. Table 2 shows the eigenvalues of each linear discriminant and the amount of between-class variance explained by each of the discriminants relative to the variance that can be explained by all discriminants.

As the first two discriminants contribute more than 99% to the between-class variability, the projected quenching efficiencies can be visualized in two dimensions. Figure 7(a) depicts the clustering along the first two discriminant functions including detection limits derived from the overlap of classes and from the deviations from the baseline. To investigate if the class separation was optimal, we checked the theoretical requirements for the LDA: normality of the quenching efficiencies and equality of the covariance matrices. Therefore, we analysed the QQ graph in figure 7(b). The good agreement to the bisecting line confirmed the normality of the input data. Out of the 1200 observations, there are just seven outliers mainly belonging to the undetectable BP. The LDA is not meaningfully affected if they are neglected. In

addition, a Bartlett test was applied on a 0.05 significance level. The test did not reject the hypothesis of equal covariance matrices (see supporting information S11). We further computed the Wilks' lambda to assess the significance of each linear discriminant on a 0.05 level. It turned out that the differences among the classes are significant with respect to all discriminant functions (see supporting information S12). However, only the first two functions strongly affect the class separation. This is in line with the observed amount of between-class variability provided by each linear discriminant shown in table 2.

In principle, the computed LDA is able to separate the investigated classes optimally. Only the data in the classes 1 ppb BP, 3 ppb BP and 10 ppb BP partly overlap with 1 ppb NB. Therefore, these four classes cannot be detected reliably. This is consistent with the quenching efficiencies for BP that do not deviate from the baseline and with those for 1 ppb NB that are very close to the baseline (see supporting information figures S12 and S15). In contrast, DNB and DNT are nicely separable following two different pathways for higher concentrations. On the first glance however, it seems that higher NB concentrations could overlap with DNT because 10 ppb NB is projected rather close to 1 ppb DNT. However, if the third linear discriminant function is taken into account, all nitroaromatics move along a different pathway (see supporting information S13). This indicates that the overall nitroaromatic separation quality further increases with increasing concentrations. Hence, not only the identification of a target analyte is possible but also the quantification of its concentration, at least for the three investigated nitroaromatics above detection limits.

To assess the LDA robustness towards out-of-sample observations, we applied the leave-one-out method. Here, the LDA was recomputed for each data point with 1199 observations while the remaining observation was used for a prediction. We only found

a few misclassifications from observations below detection limit yielding an excellent discriminatory ability with a total misclassification rate of 1.1%. For the subset validation, we used half of the data for LDA training while the other half was used for predictions. Here, we found a total misclassification rate of only 0.8%. The confusion matrices for both validation methods are given in the supporting information S14–S15.

To improve the performance of the optoelectronic nose in terms of detectable targets and classification reliability, the variety of sensor polymers could be extended by using materials with a higher spread in LUMO energies as well as in adsorption and diffusion properties. A high discrimination quality for very early and repeated responses could be achieved by a reduction of the sensor film thicknesses during printing because response times and recovery abilities would improve. However, this would decrease the signal-to-noise ratio due to lower fluorescence intensities. Additionally, novel pattern recognition approaches based on neural networks or other deep learning methods might be helpful for complex detection tasks such as the identification and quantification of single nitroaromatic species out of vapour mixtures.

4. Conclusion

We successfully demonstrated the reproducible fabrication of a printed optoelectronic nose for the selective trace detection of nitroaromatic species by digital printing of commercially available conjugated polymers. The small sensor sizes allowed for a high integration while the low standard deviations validated the within-batch reproducibility. Furthermore, we were able to demonstrate low detection limits around 1–3 ppb close to those of specially trained canines. Most importantly, the sensor arrays showed excellent discriminatory ability for nitroaromatic species using classifiers computed from LDA. Due to the excellent statistics, we have demonstrated that these classifiers are appropriate for optimal separation. The total misclassification rates of approximately 1% for out-of-sample observations underline the reliability of these classifiers. Thus, we believe that our approach opens the way for high-volume optoelectronic nose applications realizable by digital printing techniques.

Acknowledgments

We gratefully acknowledge funding from the German Federal Ministry of Education and Research (BMBF) through grant FKZ 13N13691 and from the Karlsruhe School of Optics & Photonics (KSOP). The authors declare no conflicts of interest.

References

- [1] Toal S J and Trogler W C 2006 Polymer sensors for nitroaromatic explosives detection *J. Mater. Chem.* **16** 2871–83
- [2] Rochat S and Swager T M 2013 Conjugated amplifying polymers for optical sensing applications *ACS Appl. Mater. Interfaces* **5** 4488–502
- [3] Thomas S W, Joly G D and Swager T M 2007 Chemical sensors based on amplifying fluorescent conjugated polymers *Chem. Rev.* **107** 1339–86
- [4] Wang Y, La A, Ding Y, Liu Y and Lei Y 2012 Novel signal-amplifying fluorescent nanofibers for naked-eye-based ultrasensitive detection of buried explosives and explosive vapors *Adv. Funct. Mater.* **22** 3547–55
- [5] Rupke A, Palma-Cando A, Shkura E, Teckhausen P, Polywka A, Gorrn P, Scherf U and Riedl T 2016 Highly sensitive gas-phase explosive detection by luminescent microporous polymer networks *Nat. Sci. Rep.* **6** 29118
- [6] Caron T, Guillemot M, Montmeat P, Veignal F, Perraut F, Prene P and Serein-Spirau F 2010 Ultra trace detection of explosives in air: development of a portable fluorescent detector *Talanta* **81** 543–8
- [7] Caygill J S, Davis F and Higson S P J 2012 Current trends in explosive detection techniques *Talanta* **88** 14–29
- [8] Albert K J and Walt D R 2000 High-speed fluorescence detection of explosives-like vapors *Anal. Chem.* **72** 1947–55
- [9] Woodka M D, Schnee V P and Polcha M P 2010 Fluorescent polymer sensor array for detection and discrimination of explosives in water *Anal. Chem.* **82** 9917–24
- [10] Sohn H, Sailor M J, Magde D and Trogler W C 2003 Detection of nitroaromatic explosives based on photoluminescent polymers containing metalloles *J. Am. Chem. Soc.* **125** 3821–30
- [11] Peveler W J, Roldan A, Hollingsworth N, Porter M J and Parkin I P 2016 Multichannel detection and differentiation of explosives with a quantum dot array *ACS Nano* **10** 1139–46
- [12] Cho J, Anandakathir R, Kumar A, Kumar J and Kurup P U 2011 Sensitive and fast recognition of explosives using fluorescent polymer sensors and pattern recognition analysis *Sensors Actuators B* **160** 1237–43
- [13] Hughes A D, Glenn L C, Patrick A D, Ellington A and Anslyn E V 2008 A pattern recognition based fluorescence quenching assay for the detection and identification of nitrated explosive analytes *Chem. Eur. J.* **14** 1822–7
- [14] Diehl K L and Anslyn E V 2013 Array sensing using optical methods for detection of chemical and biological hazards *Chem. Soc. Rev.* **42** 8596–611
- [15] Shanmugaraju S, Joshi S A and Mukherjee P S 2011 Fluorescence and visual sensing of nitroaromatic explosives using electron rich discrete fluorophores *J. Mater. Chem.* **21** 9130–8
- [16] Meaney M S and McGuffin V L 2008 Investigation of common fluorophores for the detection of nitrated explosives by fluorescence quenching *Anal. Chim. Acta* **610** 57–67
- [17] Geng Y, Ali M A, Clulow A J, Fan S, Burn P L, Gentle I R and Shaw P E 2015 Unambiguous detection of nitrated explosive vapours by fluorescence quenching of dendrimer films *Nat. Commun.* **6** 1–8
- [18] Kose M E, Harruff B A, Lin Y, Veca L M, Lu F and Sun Y P 2006 Efficient quenching of photoluminescence from functionalized single-walled carbon nanotubes by nitroaromatic molecules *J. Phys. Chem. B* **110** 14032–4
- [19] Hu Z, Deibert B J and Li J 2014 Luminescent metal-organic frameworks for chemical sensing and explosive detection *Chem. Soc. Rev.* **43** 5815–40
- [20] Germanenko I N, Li S and El-Shall M S 2001 Decay dynamics and quenching of photoluminescence from silicon nanocrystals by aromatic nitro compounds *J. Phys. Chem. B* **105** 59–66
- [21] Nagarkar S S, Joarder B, Chaudhari A K, Mukherjee S and Ghosh S K 2013 Highly selective detection of nitro explosives by a luminescent metal-organic framework *Angew. Chem., Int. Ed. Engl.* **52** 2881–5

- [22] Germain M E and Knapp M J 2009 Optical explosives detection: from color changes to fluorescence turn-on *Chem. Soc. Rev.* **38** 2543–55
- [23] Sun X, Wang Y and Lei Y 2015 Fluorescence based explosive detection: from mechanisms to sensory materials *Chem. Soc. Rev.* **44** 8019–61
- [24] Yang J S and Swager T M 1998 Porous shape persistent fluorescent polymer films: an approach to TNT sensory materials *J. Am. Chem. Soc.* **120** 5321–2
- [25] Askim J R, Mahmoudi M and Suslick K S 2013 Optical sensor arrays for chemical sensing: the optoelectronic nose *Chem. Soc. Rev.* **42** 8649–82
- [26] Bocksrocker T, Preinfalk J B, Asche-Tauscher J, Pargner A, Eschenbaum C, Maier-Flaig F and Lemmer U 2012 White organic light emitting diodes with enhanced internal and external outcoupling for ultra-efficient light extraction and Lambertian emission *Opt. Express* **20** A932–40
- [27] Fischer B, Kreissl S, Boeffel C and Wedel A 2012 Multi-layer printing of OLEDs as a tool for the creation of security features *Opt. Express* **20** A219–23
- [28] Ha J, Park S, Kim D, Ryu J, Lee C, Hong B H and Hong Y 2012 Solution processed polymer light-emitting diodes with single layer graphene anode *Proc. SPIE* **8476** 84760Y
- [29] Preinfalk J B, Schackmar F R, Lampe T, Egel A, Schmidt T D, Brütting W, Gomard G and Lemmer U 2016 Tuning the microcavity of organic light emitting diodes by solution processable polymer–nanoparticle composite layers *ACS Appl. Mater. Interfaces* **8** 2666–72
- [30] Liu X, Klinkhammer S, Sudau K, Mechau N, Vannahme C, Kaschke J, Mappes T, Wegener M and Lemmer U 2012 Ink-jet-printed organic semiconductor distributed feedback laser *Appl. Phys. Express* **5** 072101
- [31] Brenner P, Fleig L M, Liu X, Welle A, Bräse S and Lemmer U 2015 Degradation mechanisms of polyfluorene-based organic semiconductor lasers under ambient and oxygen-free conditions *J. Polym. Sci. B* **53** 1029–34
- [32] Yang Y, Turnbull G A and Samuel I D W 2010 Sensitive explosive vapor detection with polyfluorene lasers *Adv. Funct. Mater.* **20** 2093–7
- [33] Lindh E M, Sandström A, Andersson M R and Edman L 2016 Luminescent line art by direct-write patterning *Light: Sci. Appl.* **5** e16050
- [34] Ullah M, Tandy K, Yambem S D, Aljada M, Burn P L, Meredith P and Namdas E B 2013 Simultaneous enhancement of brightness, efficiency, and switching in RGB organic light emitting transistors *Adv. Mater.* **25** 6213–8
- [35] Meaney M S and McGuffin V L 2008 Luminescence-based methods for sensing and detection of explosives *Anal. Bioanal. Chem.* **391** 2557–76
- [36] Johnston J M, Williams M, Waggoner L P, Edge C C, Dugan R E and Hollowell S F 1998 Canine detection odor signatures for mine-related explosives *Proc. SPIE* **3392** 490
- [37] Harper R J, Almirall J R and Furton K G 2005 Identification of dominant odor chemicals emanating from explosives for use in developing optimal training aid combinations and mimics for canine detection *Talanta* **67** 313–27
- [38] Henrion R and Henrion G 1995 *Multivariate Datenanalyse* (Berlin: Springer) (<https://doi.org/10.1007/978-3-642-57792-5>)
- [39] Everitt B S and Dunn G 1991 *Applied Multivariate Data Analysis* (London: Edward Arnold) pp 320–1
- [40] Bartlett M S 1937 Properties of sufficiency and statistical tests *Proc. R. Soc. A* **160** 268–82
- [41] Narsky I and Porter F C 2013 *Statistical Analysis Techniques in Particle Physics* (Weinheim: Wiley-VCH Verlag GmbH & Co. KGaA) pp 221–7
- [42] Nagarkar S S, Desai A V, Samanta P and Ghosh S K 2015 Aqueous phase selective detection of 2, 4, 6-trinitrophenol using a fluorescent metal–organic framework with a pendant recognition site *Dalton Trans.* **44** 15175–80
- [43] Pitts J N Jr, Letsinger R L, Taylor R P, Patterson J M, Recktenwald G and Martin R B 1959 Photochemical reactions of benzophenone in alcohols *J. Am. Chem. Soc.* **81** 1068–77
- [44] Dinda D, Gupta A, Shaw B K, Sadhu S and Saha S K 2014 Highly selective detection of trinitrophenol by luminescent functionalized reduced graphene oxide through FRET mechanism *ACS Appl. Mater. Interfaces* **6** 10722–8
- [45] Nanoniele 2016 (www.nanoniele.jp/cgi-bin/nanoniele.cgi?inputsite=nanoniele_cas&keyword=119-61-9)
- [46] Li Y, Liu K, Li W J, Guo A, Zhao F Y, Liu H and Ruan W J 2015 Coordination polymer nanoarchitecture for nitroaromatic sensing by static quenching mechanism *J. Phys. Chem. C* **119** 28544–50
- [47] Ali M A, Geng Y, Cavaye H, Burn P L, Gentle I R, Meredith P and Shaw P E 2015 Molecular versus exciton diffusion in fluorescence-based explosive vapour sensors *Chem. Commun.* **51** 17406–9
- [48] Ali M A, Shoaee S, Fan S, Burn P L, Gentle I R, Meredith P and Shaw P E 2016 Detection of explosive vapors: the roles of exciton and molecular diffusion in real-time sensing *ChemPhysChem* **17** 3350–3